Torque Fluctuations In The Framework Of A Multifractal 23/9-Dimensional Turbulence Model

2014 J. Phys.: Conf. Ser. 555 012038

(http://iopscience.iop.org/1742-6596/555/1/012038)

Torque Fluctuations In The Framework Of A Multifractal 23/9-Dimensional Turbulence Model

G. Fitton[1], I. Tchiguirinskaia[1], D. Schertzer[1] and S. Lovejoy[2]

[1]Université Paris Est, Ecole des Ponts ParisTech, LEESU, 6-8 avenue B. Pascal, Cité Descartes, 77455, Marne-la-Vallée, France; tel.: +33 1 6415 3607, fax: +33 1 6415 3764
[2]McGill University, Physics department, 3600 University street, Montreal, Quebec, Canada

E-mail: `fittong@leesu.enpc.fr`

Abstract. We have carried out in-depth analyses of boundary-layer wind velocity data within a universal multifractal (UM) framework. Within the UM framework the statistics of a given field are characterised with the help of the three parameters α, C_1 and H. With these three parameters one fully describes the wind velocity fields up to and including the order q_D after which the divergence of statistical moments intervenes. Studies at different sites have shown that the parameter α – the multifractality index – of the horizontal and vertical shears of the horizontal wind remains fairly constant at approximately 1.7. In this study we show how the two remaining parameters C_1 and H vary for two very different sites/datasets and discuss what the consequences of this variability are for the fluctuations of the torque.

1. Introduction

Modern wind turbines operate in the near-surface part of the atmospheric boundary-layer i.e. between 50 to 200m above ground level. An improved understanding of turbulence-induced complexities inherent in this region therefore holds central importance for the wind energy community ([9] and [10]). To understand such complexities, accurate wind measurements at these heights require expensive and non-traditional instrumentation. This has led to insufficient amounts of adequate experimental data. At present, wind speed observations at 10m heights from meteorological networks are used in conjunction with the standard similarity theory ([20]). The use of such methods does not fully represent the complexity of the vertical profile of the wind.

Within the so called surface-layer there exist highly complex three-dimensional time-dependent turbulent fields involving multi-scale structures whose non-linear interactions and statistics evolve with the turbulence generation mechanism. Moreover, these turbulent structures change drastically when generated mostly by buoyancy forces compared to those generated by wind shear (see [18]). This is partially in agreement with the (isotropic) scaling 'buoyancy sub-range' hypothesised by Bolgiano-Obukhov ([3, 22]) hereafter referred to as BO.

In addition to the complexities involved in changing turbulence generation mechanisms further complexities arise when inhomogeneous terrains are involved. To take advantage of the wind speed-up induced by eddies forced up over a hill, turbines are frequently installed on hilltops. This is done even though there is only a limited amount of knowledge concerning the mechanisms responsible for the complex fluid dynamics that occur on the upwind side of the

hill ([11]). What's more, if the upwind side of the hill contains tall vegetation the turbulent structures and atmospheric stability will be *even* further modified ([5]).

Removing the effects of a complex terrain i.e. when the surface satisfies a horizontally homogeneous terrain assumption, does not make the problem much simpler. A low-level jet phenomena occurring between 50 to 400m can also cause reason for concern ([1, 2]). In summary, to establish a reference of the observable space-time variability of wind-inflow events, in particular of extreme wind speed gusts, very detailed observations need to be made in a variety of locations and situations.

The wind energy community defines as 'extreme', those wind-inflow events, that can potentially produce, adverse, damaging impacts on modern wind turbines (see [9] and [10] for a review). This includes events such as: persistent wind gusts, rapid changes in wind direction, and atmospheric coherent structures; events that are likely to generate critical loads on wind turbines. If these events occur too frequently the wind turbine will prematurely fatigue. It is thus of vital importance that the (statistical) predictions of the extreme wind-inflow events are improved. Improved predictions of the wind turbine loads will help to develop advanced generator torque controls, thus minimising the potential damage caused by extreme wind events.

The significance of turbulence intensity on the optimal torque control gain for different time scales was investigated in [12]. The so called 'turbulence intensity', deeply rooted in the Reynolds decomposition, is defined as the standard deviation of the wind speed, normalised by the mean wind speed over a given interval of time. Within the wind energy community this time interval is typically from 10 minutes to one hour. Bearing in mind an active torque control must be responsive down to time scales comparable to the transition time of a few seconds – in order to mitigate the impact of extreme events – it is unlikely the study of such coarse time-scales could be truly representative of the variability in the system. Moreover, because the turbulence intensity is defined through the mean and therefore framework dependent velocity, the normalisation does not respect Galilean invariance. A tool that has been fundamental in the understanding of the multi-scale structures in turbulence is ironically lost in a term claiming to be that which it least describes. And yet, in spite of these facets, the turbulence intensity is still widely used as a classical measure of the 'gustiness' of the wind.

In light of these problems (and opportunities), current atmospheric and therefore torque measurements can be analysed using modern statistical methods. Statistical methods that are appropriate to the study of events considered to be extreme by the wind energy community. This paper argues that the current focus of research in wind resource assessment should be devoted to the multifractal modelling of atmospheric turbulence. A model that, instead of performing scale-by-scale developments in the design of separate features of a wind turbine, aims to integrate knowledge across the spatio-temporal scales.

Multifractals are space or space-time fields that have scale invariant structures at all scales. Their power law statistics therefore do not depend on the scale of observation. This allows us to understand and to model extremely variable space-time fields over a wide range of scales. At present one would expect the wind energy community to go beyond the Reynolds decomposition. This means taking into account the fundamental problem of intermittency and addressing the fact that the so-called 'mean' wind is frame dependent.

2. Intermittency And The Physics Of Extremes

Intermittency means that the activity of a process is confined to smaller and smaller fractions of the available space-time domain when observed at higher and higher resolutions. We define the resolution, λ, as the ratio of the largest scale, L, and the reference scale, ℓ (λ is therefore dimensionless). Examples of intermittency can easily be observed in wind farm wind velocity data. Figure 1 illustrates a twenty-second time-series of the wind velocity fluctuations, $\Delta u_x = u_x(t+\tau) - u_x(t)$ (i.e., the velocity fluctuations along the horizontal x-axis), from Corsica

(France) with $\lambda = 200$. The velocity increments show a highly variable process with sporadically occurring extreme values. Moreover, because the flux of energy at a given ratio of scales, ε_λ, is proportional to the third power of the wind velocity increment, will vary by orders of magnitude in time and in space. The highest values of the flux at any given scale relative to the mean, increase with increasing Reynolds number. These values could easily therefore be of an order fifteen times greater than the average energy flux in laboratory scale flows and fifty times that of the average energy flux in atmospheric flows.

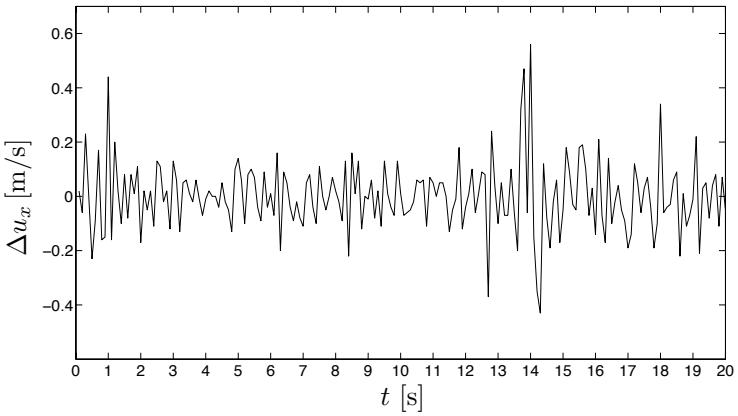

Figure 1: Twenty second time-series of wind velocity increments for the horizontal u_x-component of the Corsica dataset. The sporadic nature of the large fluctuations is characteristic of an intermittent process.

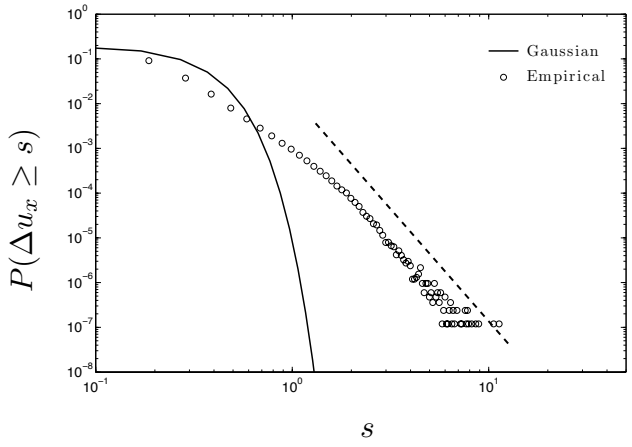

Figure 2: Log-log plot of the probability of exceedance, $P(\Delta u_x \geq s)$, of the (normalised) velocity increments, Δu_x, of the twenty second time-series in figure 1. The slope of the dashed line is 6 i.e. $q_D = 6$. This means velocity increment statistics above an order of 6 are random, i.e., statistical moments of order larger than 6 are no longer numbers, but random variables that fluctuate with samples; there is no longer convergence to a given number (the theoretical statistical moment) with increasing sample size.

The irregular nature of the large fluctuations characteristic of an intermittent process will often result in the divergence of statistical moments (see figure 2). The divergence of statistical

moments of a random variable correspond to a 'hyperbolic' (algebraic) fall-off of the probability distribution tail

$$P(\Delta u_x \geq s) \approx s^{-q_D} \implies \langle \Delta u_x^q \rangle = \infty, \ q > q_D \tag{1}$$

where s is a threshold of intensity with a tail exponent of critical order q_D. With respect to the scaling moment function discussed below, the critical order $q_D > 1$ is the solution of $K(q_D; 1) = (q_D - 1)D$. The exponent characterises the relative frequency of extreme events i.e. extremes are more frequent when the exponent q_D is smaller. This statistical behaviour is a consequence of the fact that the sum of the contributions is dominated by the strongest contribution; rare events have a dominant contribution ([23]). For the statistical moments of order $q < q_D$ the wind velocity increments correspond to a non-linear form of the structure-function exponent $\zeta(q) = q/3 - K(q; 1/3)$. The scaling moment function $K(q; 1/3)$ characterises the intermittency of the velocity field.

3. Multifractal Behaviour Of Wind Velocity Shears

Over the past two years we have carried out two in-depth analyses of boundary-layer wind velocity data within a universal multifractal (UM) framework [23]. In a very general manner, multifractals are space-time fields that have structures at all scales. The wind velocity field is turbulent and strongly variable over a wide range of scales. The turbulence in the atmosphere is produced by an outer force, giving rise to kinetic energy at large scales, transferred to smaller scales without dissipation until the terms of viscosity can no longer be neglected. Then the conservative energy flux can be modelled in a multiplicative way from one scale to the next smaller scale, while at the same time becoming more and more intermittent. The small scale limit of such multiplicative cascade gives rise to a multifractal field, ε_λ, whose statistical moments are defined by a non-linear scaling moment function

$$\langle \varepsilon_\lambda^q \rangle \approx \lambda^{K(q;1)}. \tag{2}$$

Within this framework we consider that the wind shears scale as

$$\Delta u_\lambda \stackrel{d}{=} \varepsilon_\lambda^a \lambda^{-H}, \tag{3}$$

where $\stackrel{d}{=}$ denotes equal in distribution, H is a scaling exponent and a is the power of the flux. Whereas the energy flux is a conservative quantity, which means that its statistical average is scale independent, the scaling exponent H measures the non-conservativeness of the velocity field. Moreover, depending on whether the energy flux or the force variance flux is conserved one may consider that the buoyancy force variance flux, ϕ, plays the same role as the energy flux, ε, in 3D turbulence but only along the vertical:

$$\Delta u(\Delta x) \stackrel{d}{=} (\varepsilon(\Delta x))^{1/3} \Delta x^{1/3} \text{ and } \Delta u(\Delta z) \stackrel{d}{=} (\phi(\Delta z))^{1/5} \Delta z^{3/5}. \tag{4}$$

Within the UM framework the statistical moments of a given field are characterised with the help of a limited number of parameters: α, C_1, a and H. For a conservative field ($H = 0$) the scaling moment function reads as

$$K(q; a) = a^\alpha \frac{C_1}{\alpha - 1} \left(q^\alpha - q\right) \tag{5}$$

for $q < q_D$. In order to estimate the parameters α and C_1 we use the double trace moment method ([16] and [24] for a review). When the origin of the flux and hence its power, a, remains unknown, the estimate of C_1 on velocity fluctuations absorbs the pre-factor and hence C_1 becomes slightly α-dependent.

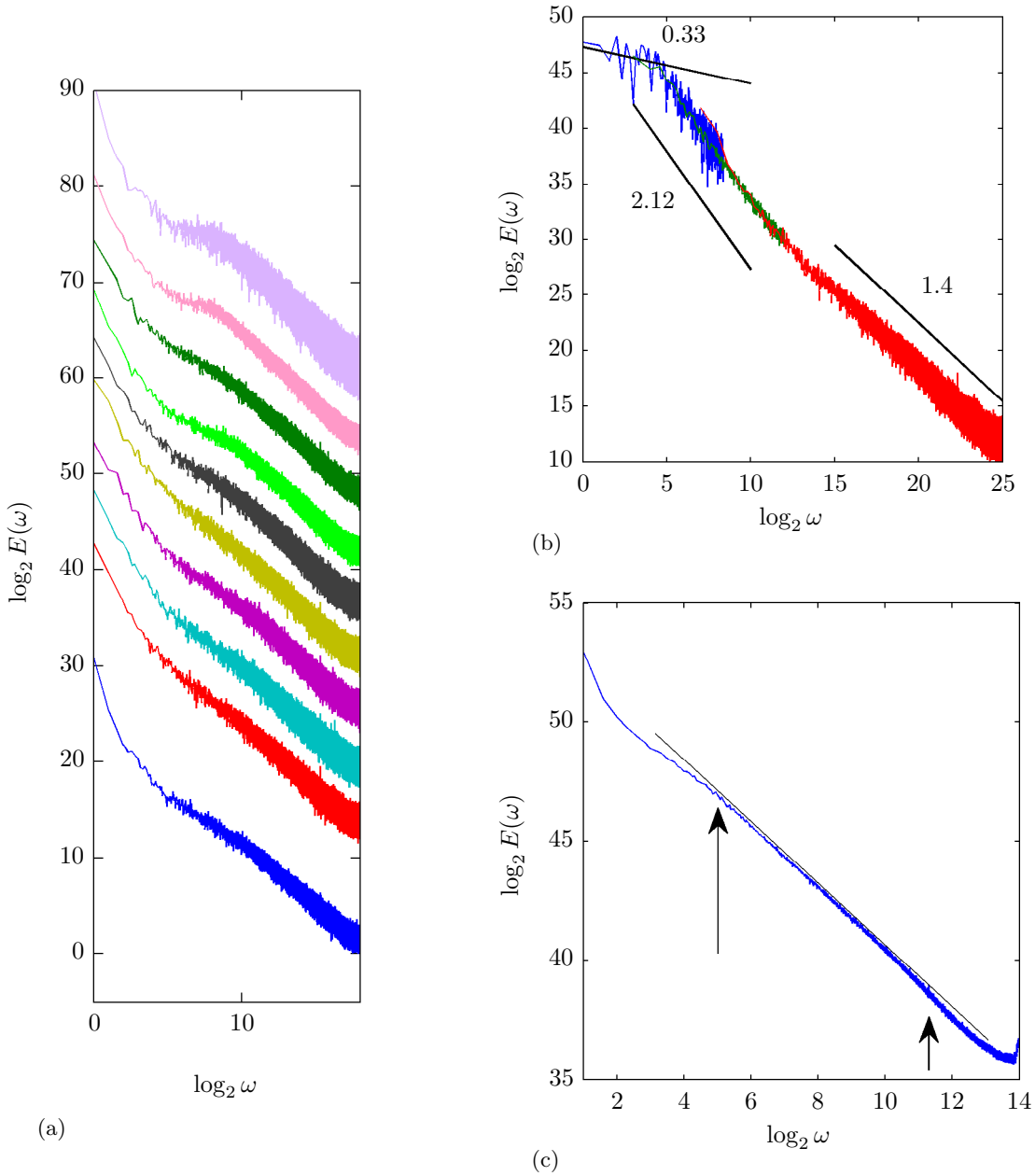

Figure 3: Plots of averaged u_x-component wind velocity spectra ($E_u(\omega)$) at a 43m height versus the normalised frequency, ω. The frequency is normalised such that $\omega = 2^N/\ell_n = \lambda/0.1\text{s}$, where $\ell_n = 2^n \times 0.1\text{s}$ for $n \in [0:N]$ and $N = 19$, 25 and 14 for (a), (b) and (c) respectively. (a) Spectra, $E_u(\omega)$, for meteorological varying wind directions (see text) shifted vertically for clarity from bottom to top; (b) The spectra assumed to have the least influence from the turbine (the second red plot) is compared with even lower frequency spectra achieved by concatenating each daily sample into a larger continuous file. The largest concatenation consists of about 100 files giving a maximum ratio of scales, $\lambda = 2^{25}$ (blue). The higher frequencies of the concatenated files have been removed to give a continuously scaling appearance; (c) Inversely each daily sample can be split into sub-samples and averaged in order to get smoother scaling over the higher frequencies. The slope of the line of best fit is 1.35.

The non-conservativeness parameter H is estimated through spectral analysis. The Fourier transform of the second-order-moment structure function yields the energy spectrum $E(\omega) \propto \omega^{\beta}$, where the scaling exponent $\beta = 2H + 1 - K(2; a)$. Note, using the first order structure-function will give the same result provided the same ranges of scales are used in the regression procedure.

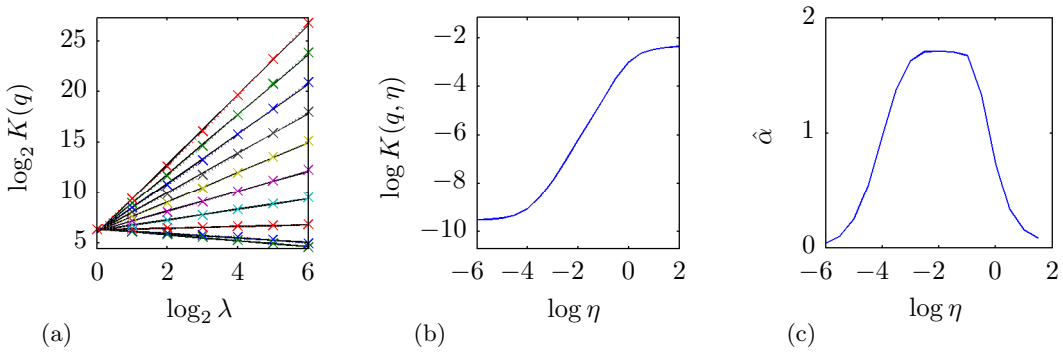

Figure 4: (a) Ensemble average of trace moments for $q = 1.5$ and $\log \eta \in [-6 : 2]$; (b) resulting double trace moment curve; (c) the local estimate $\hat{\alpha} = \Delta \log K(q, \eta)/\Delta \log \eta$, of α. The trace moments are estimated on the energy flux over the mid-frequency sub-range (the green plot from figure 3b) of the Corsica dataset. The parameters over these time-scales are: $\alpha = 1.67, C_1 = 0.56$ and $H = 0.64$.

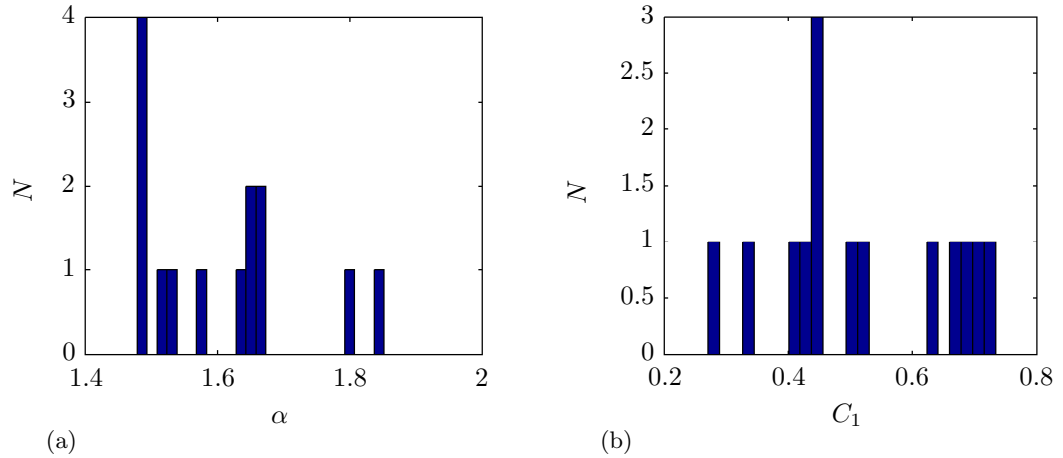

Figure 5: Distribution of UM parameters α (a) and C_1 (b) estimated on the energy flux of the Corsica dataset over the frequencies $\log_2 \omega \in [5 : 12]$. Estimates of $\alpha = 2$ and the corresponding C_1s have been removed leaving a total of 14 samples from 80.

Figure 3 displays log-log plots of the averaged u_x-component wind velocity spectra at 43m from the Corsica dataset. The Corsica dataset consists of high-resolution (10Hz) ultrasonic wind anemometer data taken over six-months. The measurements were taken at 22, 23 and 43m above the ground in a wind farm test site subject to complex terrain and buoyancy forces from the nearby sea. Very often, as in the Corsica dataset, only time-series measurements of the velocity are available from an anemometer in a fixed position r say. By Taylor's frozen turbulence hypothesis ([26]) we can consider $u_x(x, t + \tau) = u_x(x - U\tau, t)$, where U is the mean (advecting)

wind. Hence, the spectral exponent is still expected to be close to the Kolmogorov-Obukhov (KO) inertial range 5/3s value.

Figure 3a shows the average (over ten samples for each mean direction) of spectra for meteorological wind directions, $\theta_{\rm met}$ = 9, 35, 62, 86, 116, 134, 162, 188, 210, 238, 260 and 281 degrees. The direction, $\theta_{\rm met}$, is where the wind is coming from with respect to true North e.g. 0° is North, 90° is East etc. Due to the effects resulting from the wakes of the turbine it was important to find a control sample from which to observe undisturbed scaling behaviour. Based on the spectra with the least amount of fluttering i.e. the least influence from the turbine (see figure 3 for details), the samples are then compared with even lower frequency spectra (see [7]). This is achieved by concatenating each individual sample (measured continuously over a day) into a larger continuous file. The largest concatenation consists of about 100 files giving a maximum ratio of scales, $\lambda = 2^{25}$ (figure 3b blue). The higher frequencies of the concatenated files have been removed to give a continuously scaling appearance.

Based on the pseudo-continuously scaling plot we can see there exist three distinct scaling sub-ranges. Over the lowest frequencies ($\log_2 \omega \in [0:5]$) of figure 3b we have a scaling exponent that is comparable with low frequency 'macro' weather (see [17]). This is then adjoined by an apparent BO scaling region over the frequencies $\log_2 \omega \in [5:12]$. And finally, for the frequencies $\log_2 \omega \in [12:25]$ we observe something close to KO scaling. Over this high frequency KO scaling sub-range the spectra are fairly noisy. We can improve the statistics over the higher frequencies in an inverse fashion to the concatenation for very low frequencies. That is, each daily sample can be split into sub-samples and the resulting spectra then averaged. Figure 3c displays the result of this procedure.

Figures 4a, b and c show: the trace moments for $q = 1.5$ and $\log \eta \in [-6:2]$, the resulting double trace moment curve and the local estimate ($\hat{\alpha}$) of α, all estimated on the energy flux over the mid-frequency sub-range ($\log_2 \omega \in [5:12]$, see 3b) of the Corsica dataset. The trace moments show the data scale well if the ensemble average are used. This gives an extended range of $\log \eta$ i.e. $\log \eta \in [-3:-1]$ over which α is constant. The corresponding UM parameters are $\alpha = 1.67$ and $C_1 = 0.56$. Over the high-frequency range $\alpha = 1.66$ and $C_1 = 0.23$. Using equation 5 we get $H = 0.64$ over the mid-frequency range and $H = 0.23$ over the high-frequency range, with intermittency corrections $K(2;1/3) = 0.16$ and 0.06 respectively (see equation 5).

Because the ensemble averaged trace moments give a more stable result we do not have error bars on the estimates. Figure 5 gives an idea of the dispersion of the individual estimates of the UM parameters.

Figure 6a displays a log-log plot of the averaged horizontal u_x-component spectra at 50m from the Growian dataset. The Growian experiment in Germany consisted of an array of cup anemometers recording horizontal wind speeds at 2.5Hz [15]. The array formed a grid of approximately 75 by 100m, with the lowest point being at 50m. This was comparable, in part, to the heights of the measurements taken in Corsica. However, due to the spatial distribution of the measurements, unlike in Corsica, we were able to test if the scaling laws were valid in space and in time [26]. For the Growian dataset the wind speed and direction are provided and the corresponding horizontal wind vectors are decomposed such that $u_x = u \cdot \cos\theta$ and $u_y = u \cdot \sin\theta$. For this study we selected a system of coordinates such that $\langle u_y \rangle = 0$ in order to impose 'mirror symmetry' as suggested in ([13]).

The velocity spectra exhibit scaling over two sub-ranges: approximately $\log_2 \omega \in [1:7]$ and [7:10]. Over the lower frequency sub-range there is a scaling exponent $\beta = 1.2$. Over the higher frequency sub-range the scaling exponent falls closer to homogeneous KO scaling with $\beta = 1.7$. The UM parameters over both low and high frequencies are the same i.e.: $\alpha \approx 1.8$ and $C_1 \approx 0.7$. This gives an intermittency correction $K(2;1/3) = 0.18$ and therefore $H = 0.19$ and 0.44 over low and high-frequency sub-ranges respectively. The scaling of the spectra is consistent with that observed in [14] in which a -1 energy production scaling sub-range is adjoined by a KO

scaling sub-range. Although this scaling behaviour is observable close to the ground we find with increasing height (figure 6b) the processes become mixed and the scaling exponents deviate from the two predicted adjoining sub-ranges.

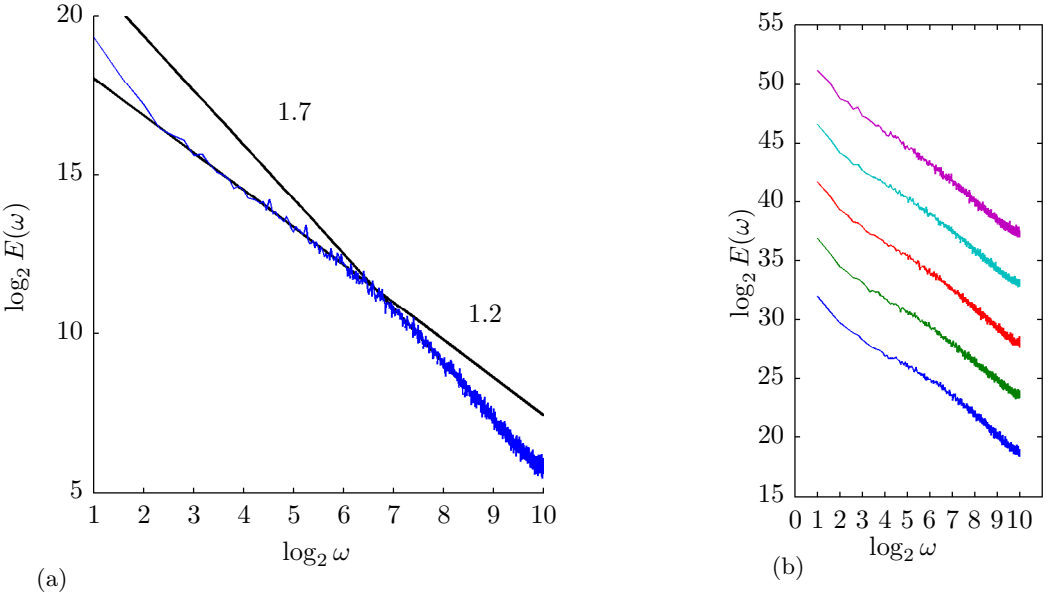

Figure 6: (a) Log-log plot of average horizontal wind speed spectra, $E_{u_x}(\omega)$, at 50m from the Growian dataset. The frequency is normalised such that $\omega = 2^N/\ell_n = \lambda/0.4\text{s}$, where $\ell_n = 2^n \times 0.4\text{s}$ for $n \in [0:N]$. The spectral slopes (black solid lines) are 1.2 over low frequencies ($\log_2 \omega \in [1:7]$) and 1.7 is over high frequencies ($\log_2 \omega \in [7:10]$); (b) Spectra of $E_{u_x}(\omega)$ at 50, 75, 100, 125 and 150m (from bottom to top [shifted for clarity]). Corresponding spectral slopes over higher frequencies are: 1.77, 1.58, 1.64, 1.56 and 1.51, and over lower frequencies are: 1.12, 1.24, 1.25, 1.28 and 1.39.

4. Scaling Anisotropy And The Implications For The Torque Fluctuations

4.1. Scaling Anisotropy

The Generalised Scale Invariance (GSI) approach posits scale invariance (scaling) as the main symmetry and then considers the remaining non-trivial symmetries. These symmetries are generally no longer isotropic (see [25] for details). The anisotropy exponent, H_z, measures the deviation of scaling laws (self-similarity) from isotropy between two directions. For example, when taking the horizontal and vertical shears of the horizontal wind, $H_z = H_h/H_v = C_{1,h}/C_{1,v} = 5/9$. The subscripts h and v correspond to two different scaling relations (equation 4). This corresponds to the multifractal 23/9-dimensional turbulence model.

When using time-series measurements, the dominant role of the vertical motion of large scale atmospheric structures may explain (e.g., [7]) why BO scaling becomes apparent over the range of corresponding frequencies. For the Corisca dataset we find that $H_h/H_v = 0.23/0.64 = 0.36$ and $C_{1,h}/C_{1,v} = 0.22/0.56 = 0.39$ which thus (indirectly) validates the anisotropic model of the wind shears (although with a lower anisotropy exponent $H_z = 0.4$). For the Growian dataset, since the co-dimension remains the same for all timescales when $\langle u_y \rangle = 0$, a much simpler model can be used in which only a modification of H is required. Indeed, the wind shears become about 0.43 times (i.e., $H_z = 0.19/0.44$) less convoluted over low frequencies. Note, the test of the ratio of scaling exponents has been performed over different scales for the two datasets. We

are unable to directly compare the two datasets due to the shorter ratio of scales in the Growian dataset. If we look at similar smaller scales between the two datasets, i.e., figures 3 and 6 their scaling properties are indeed comparable in that a small-scale KO range is followed by larger scale -1 scaling law.

4.2. The Torque Fluctuations

The rotor torque for a wind turbine is given by the cross product of the thrust force F and the (gyration) radius of the blade r, i.e. $F \times r$. This implies that for unit mass, the torque, Q, and its time fluctuations, $\Delta Q(\Delta t) = Q(t + \Delta t) - Q(t)$, both have the dimensionality of a velocity squared. If furthermore ΔQ depends mainly on the velocity fluctuations Δu, as suggested by [21], and has no characteristic intensity, then:

$$|\Delta Q(\Delta t)| \stackrel{d}{=} A \Delta u_x^2(\Delta t) \tag{6}$$

where A is a given dimensionless constant. Moreover, by equations 4a and 4b, $|\Delta Q| \propto \varepsilon^{2/3}\ell^{2/3}$ and $|\Delta Q| = \phi^{2/5}\ell^{6/5}$. Using the UM parameters estimated from the two sites we can then simulate the torque fluctuations.

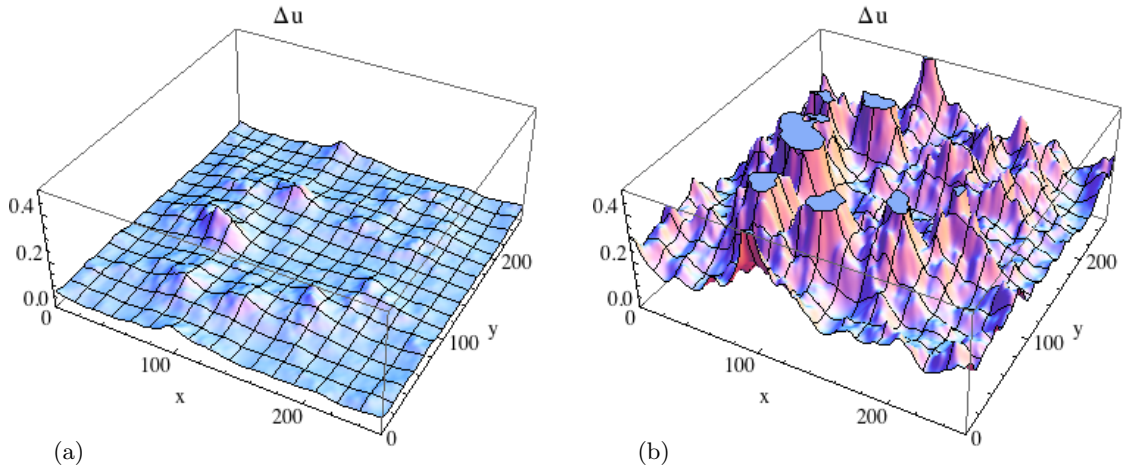

Figure 7: Two-dimensional (scalar) simulations of velocity fluctuations, Δu, for a ratio of scales $\lambda = 2^8$. Plots (a) and (b) are simulated using the Growian high and mid-frequency UM parameter estimates for the energy flux: respectively $\alpha = 1.7$, $C_{1,\varepsilon} = 0.7$ and $H = 0.44$ and $H = 0.19$. The codimension used to simulate the velocity (using $C_{1,\Delta u} = C_{1,\varepsilon}(1/3)^{\alpha}$) is then $C_{1,\Delta u} = 0.097$.

Equation 6 shows that the torque fluctuations have the same multifractality parameter, α, as the velocity fluctuations, however, the non-conservativeness parameter increases two-fold. The mean co-dimension C_1 is modified by the pre-factor $(2a)^{\alpha}$. Figures 7 and 8 display the (dimensionless) UM velocity fields together with examples of resulting torque fluctuations (figure 9). Figures 7a and 8a correspond to the velocity fluctuations resulting from an intermittent KO scaling velocity sub-range followed by a smoother sub-range (possibly a -1 power law energy production sub-range, see figure 7b) respectively. Note that the deviations from the predicted scaling exponents in both cases suggests the processes are more complex, possibly mixed. Given the vertical scales in both plots are the same we can consider that both processes result in similarly strong variability of the torque fluctuations, while the velocity increment variability is fully compatible with that displayed by figure 1. Figure 7b corresponds to a velocity field

resulting from an adjoining more convoluted sub-range predicted to follow an energy production sub-range. Figure 8b possibly corresponds to a BO process.

Comparing each of the three processes from the simulations: figures 7a and 8a for a Kolmogorov-Obukhov process, figure 7b for a -1 energy production process and 8b for a Bolgiano-Obukhov process, we can see the type of process is very important for quantifying the fluctuations. From the estimates of C_1 and H we know the processes are likely mixed between an 11/5s and a 5/3s power law with intermittency corrections. We can therefore hypothesise that it is the mixing of such processes that gives the deviation of H_z from the predicted 5/9s.

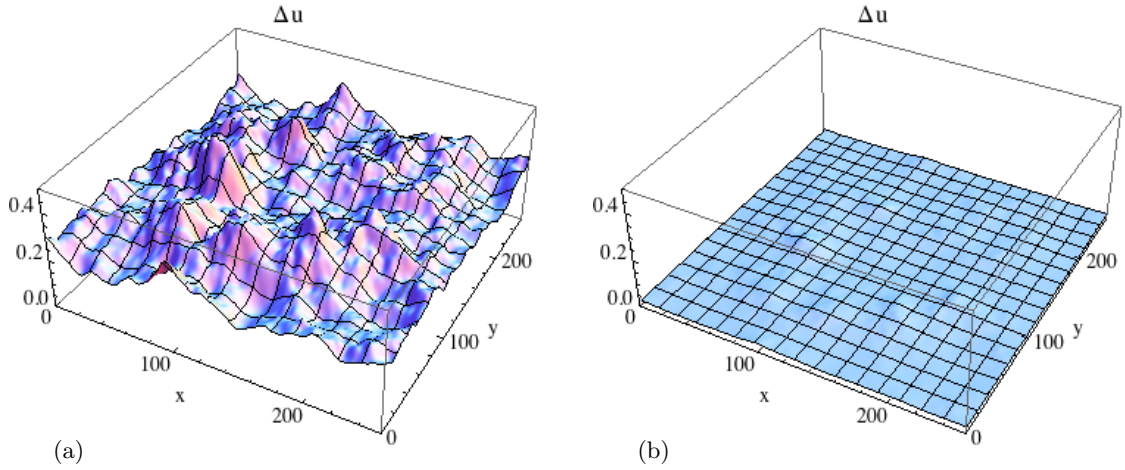

Figure 8: Two-dimensional (scalar) simulations of velocity fluctuations, Δu, for a ratio of scales $\lambda = 2^8$. Plots (a) and (b) are simulated using the Corsica high and lower-frequency UM parameter estimates for the energy flux: respectively $\alpha = 1.8$, $C_{1,\varepsilon} = 0.23$ and $H = 0.23$; and $C_{1,\varepsilon} = 0.56$ and $H = 0.64$. The codimensions used to simulate the velocity are then $C_{1,\Delta u} = 0.036$ and $C_{1,\Delta u} = 0.086$.

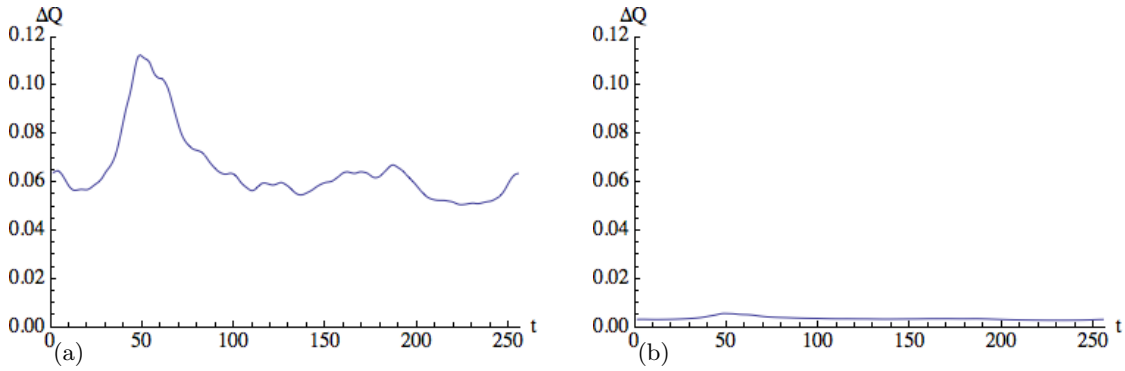

Figure 9: Time-series simulations of the torque fluctuations, ΔQ, for a ratio of scales $\lambda = 2^8$. Plots (a) and (b) are simulated using the high-frequency UM parameter estimates for the Corisca and Growian datasets. For the Corsica dataset $\alpha = 1.8$, $C_{1,\Delta Q} = 0.12$ and $H = 0.46$; For the Growian dataset $\alpha = 1.7$, $C_{1,\Delta Q} = 0.34$ and $H = 0.88$. Similalry the codimensions of the torque are computed from $C_{1,\Delta Q} = C_{1,\varepsilon}(2/3)^{\alpha}$, the Hurst parameter is simply twice that estimated for the velocity.

The drastic qualitative difference of the variability displayed by figures 8a to 8d is mainly due to the difference in value of the exponents H. Indeed, its main role is to smooth out the field by precisely decreasing the field singularities by $-H$, i.e. smoothing the spikes at resolution λ by a factor λ^H, while other UM parameters remain rather similar. This corresponds to a damping factor of $2^{8\times.9} \approx 2^7 = 128$, i.e. two orders of magnitudes, for figure 8b with respect to figure 8a. Finally, figures 9a and 8b display the (dimensionless) UM torque fluctuations resulting from the scaling of velocity fields displayed in figures 7a and 8a.

5. Concluding Remarks

Casting our minds back to figure 3a, for directions influenced by wind turbine wakes, there is a highly intermittent sub-range with a smoother spectral slope than KO that is followed by a less intermittent KO scaling sub-range (see [7] for more details). This suggests that there is an adjoining (high-frequency) range of time and therefore length-scales in which the strong velocity and therefore torque fluctuations can be smoothed depending on the process. The quantification of the effect of smoothing for different processes can be estimated with the help of the factor λ^{-H} for processes having rather similar other UM parameters. This reduction factor is also relevant for the estimation of the fatigue.

Finally, the probability tails of the Corsica dataset showed that the critical order above which statistical moments diverge is about $q_D = 6$. One of the consequences of the second order relation between the torque and the velocity increments is that for the torque fluctuations the critical exponent is therefore twice smaller than that of the velocity fluctuations. This implies that for orders larger than three the empirical statistics will display larger and larger fluctuations with increasing sample size. Consequently standard statistical methods of analysis will underestimate the extremes.

6. Acknowledgments

The authors highly acknowledge the help of Joachim Peinke who facilitated the access to the Growian dataset and Eric Dupont and Luc Musson Genon who provided access to the data of the EDF wind farm in Corsica. Their illuminating discussions help to stimulate our research. We would also like acknowledge the WAUDIT project for funding this research.

References

[1] R. Banta, R. Newsom, J. Lundquist, Y. Pichugina, R. Coulter, & L. Mahrt. (2002). Nocturnal Low-Level Jet Characteristics Over Kansas During CASES-99. Boundary-Layer Meteorology, 105(2), 221–252.
[2] R. Banta, Y. Pichugina, & R. Newsom. (2003). Relationship Between Low-Level Jet Properties And Turbulence Kinetic Energy In The Nocturnal Stable Boundary Layer. Journal of the atmospheric sciences, 60(20), 2549–2555.
[3] R. Bolgiano, (1959). Turbulent Spectra In A Stably Stratified Atmosphere. Journal Of Geophysical Research, 64(12), 2226–2229.
[4] R. Calif, F. Schmitt. (2014). Multiscaling And Joint Multiscaling Description Of The Atmospheric Wind Speed And The Aggregate Power Output From A Wind Farm. Nonlinear Processes In Geophysics
[5] J. Finnigan. (2000). Turbulence In Plant Canopies. Annual Review Of Fluid Mechanics.
[6] G. Fitton, I. Tchiguirinskaia, D. Schertzer, & S. Lovejoy. (2011). Scaling Of Turbulence In The Atmospheric Surface-Layer: Which Anisotropy? Journal Of Physics: Conference Series, 318(7), 072008.
[7] G. Fitton, I. Tchiguirinskaia, D. Schertzer, & S. Lovejoy. (2011). The Anisotropic Multifractal Model and Wind Turbine Wakes. 7th PhD Seminar on Wind Energy in Europe, 115–118.
[8] G. Fitton, I. Tchiguirinskaia, D. Schertzer, & S. Lovejoy. (2012) Wind Energy And The Impact Of Turbulence On The Conversion Process. Euromech 528 proceedings.
[9] E. Hau. (2006). Wind Turbines-Fundamentals, Technologies, Application, Economics. 2nd Edition
[10] B. Sorensen. (2007) Renewable Energy Conversion, Transmission, And Storage.
[11] J. Hunt, S. Leibovich, & K. Richards. (1988). Turbulent Wind Flow Over Smooth Hills. QJR Meteorological Society
[12] K. Johnson. (2004). Adaptive Torque Control Of Variable Speed Wind Turbines. Citeseer.

[13] B. Kader, & A. Yaglom. (1989). Spatial Correlation Functions Of Surface-Layer Atmospheric Turbulence In Neutral Stratification. Boundary-Layer Meteorology.
[14] G. Katul, & C. Chu. (1998). Boundary-Layer Meteorology, Volume 86, Number 2 - SpringerLink. Boundary-Layer Meteorology, 86(2), 279–312. doi:10.1023/A:1000657014845.
[15] F. Korber, G. Besel, & H. Reinhold. (1988). Messprogramm an der 3 MW-Windkraftanlage GROWIAN: Forderkennzeichen 03E-4512-A. Forschungsbericht / Bundesministerium fur Forschung und Technologie, Nichtnukleare Energietechnik. Grosse Windenergieanlage Bau- u. Betriebsges.
[16] D. Lavalle, S. Lovejoy, D. Schertzer, & F. Schmitt. (1992). On The Determination Of Universal Multifractal Parameters In Turbulence. Topological Aspects Of The Dynamics Of Fluids And Plasmas, 463–478.
[17] S. Lovejoy, D. Schertzer, & D. Varon. (2012). Do GCM's predict the climate. Or low frequency weather? EGU General Assembly.
[18] C. Moeng, & P. Sullivan. (1994). A Comparison Of Shear-And Buoyancy-Driven Planetary Boundary Layer Flows. Journal Of The Atmospheric Sciences.
[19] P. Milan, M. Wächter, and J. Peinke. (2013). Turbulent Character Of Wind Energy. Phys. Rev. Lett.
[20] A. Monin, & A. Obukhov. (1959). Basic Laws Of Turbulent Mixing In The Surface Layer Of The Atmosphere. Contrib Geophys Inst Acad Sci USSR151, 24(151), 163–187.
[21] T. Mücke, D. Kleinhans, and J. Peinke. (2011). Atmospheric Turbulence And Its Influence On The Alternating Loads On Wind Turbines. Wind Energy. (14) 2, 301–316
[22] A. Obukhov. (1959). Effect Of Archimedean Forces On The Structure Of The Temperature Field In A Turbulent Flow (Vol. 125, p. 1246). Presented at the Dokl. Akad. Nauk SSSR.
[23] D. Schertzer, S. Lovejoy, F. Schmitt, I. Tchiguirinskaia and D. Marsan (1997). Multifractal cascade dynamics and turbulent intermittency. Fractals 5(3): 427–471.
[24] D. Schertzer, & S. Lovejoy. (2011). Multifractals, Generalized Scale Invariance and Complexity in Geophysics. International Journal of Bifurcation and Chaos, 21(12), 3417–3456.
[25] D. Schertzer, I. Tchiguirinskaia, S. Lovejoy, & A. Tuck. (2011). Quasi-Geostrophic Turbulence And Generalized Scale Invariance, A Theoretical Reply. Atmos. Chem. Phys. Discuss, 11(1), 3301–3320. doi:10.5194/acp-12-327-2012
[26] G. Taylor. (1922). Diffusion by Continuous Movements. Proceedings of the London Mathematical Society, s2-20(1), 196–212.